DOI:10.1039/c6cp07508h

# Physical Picture for Mechanical Dissociation of Biological Complexes: from Forces to Free Energies†

Rafael Tapia-Rojo,[a‡] Carlos Marcuello,[b§] Anabel Lostao,[c] Carlos Gómez-Moreno,[b] Juan J. Mazo,[d] and Fernando Falo*[a]

Single-molecule force spectroscopy is a powerful technique based in the application of controlled forces to macromolecules. In order to relate the measured response of the molecule with its equilibrium and dynamical properties, a suitable physical picture of the involved process is necessary. In this work, we introduce a plausible model for mechanical unbinding of some molecular complexes, based on a novel free energy profile. We combine two standard theoretical frameworks for analyzing force spectroscopy experiments for two protein:protein complexes, obtaining key magnitudes of the underlying free energy profile, which are only understood within the mentioned model. Additionally, we carry out detailed stochastic dynamics simulations to prove the validity of the analysis protocol and the reliability of the free energy profile. Remarkably, we can compare directly the obtained unbinding free energies with the previously known bulk binding free energies, bridging the gap between bulk and single molecule techniques.

## 1 Introduction

Since the irruption of single molecule techniques, the study of biological processes at the molecular level has been completely revolutionized[1,2]. The possibility of manipulating individual molecules allows to sample directly distributions of molecular properties, providing the identification of rare subpopulations, something inconceivable with bulk biophysical assays, where ensemble averaging is inherent to the technique. Specifically, single molecule dynamic force spectroscopy (DFS) involves the application of controlled forces to biological macromolecules or complexes[3,4], inducing conformational changes such as unfolding of proteins[5] and nucleic acids[6], dissociation of ligand-receptor complexes[7–10] or even unravel enzyme catalysis mechanisms[11].

In this context, processes such as molecular unbinding are usually characterized by a free energy profile along a reaction coordinate, namely the pulling direction. This profile shows a single -or multiple- free energy barrier $\Delta G^\dagger$ and an unbinding or dissociation free energy $\Delta G^0$, which respectively control the kinetic and thermodynamic properties of the system. Ultimately, force spectroscopy experiments aim to access to this information by measuring rupture forces on such molecular transitions.

In the last few years, wide theoretical effort has been focused on this goal. For instance, when pulling a molecule at constant rate $r_f = df/dt$, force spectroscopy theory[12–17] relates the most probable rupture force $f^*$ with the free energy barrier height $\Delta G^\dagger$, the position of the transition state $x^\dagger$ and the intrinsic rate coefficient $k_0$. In addition, Jarzysnki equality[18] provides the free energy difference between two equilibrium states $\Delta G^0$ by measuring the work performed over a non-equilibrium transition between such states[19–21]. A combined application of both theoretical frameworks would provide a global picture of the kinetic and equilibrium characteristics of the system. Nevertheless, they should be understood together within a suitable shape of the free energy profile, concerning the particular system of study.

In this work, we study the problem of mechanical dissociation of molecular complexes[10,22–26]. Here, the force is typically exerted to the complex through a polymer linker attached to the

[a] Instituto de Biocomputación y Física de Sistemas Complejos and Departamento de Física de la Materia Condensada, Universidad de Zaragoza, 50009 Zaragoza, Spain
[b] Laboratorio de Microscopías Avanzadas, Instituto de Nanociencia de Aragón, Universidad de Zaragoza, 50018 Zaragoza, Spain; and Fundación INA, 50018 Zaragoza, Spain.
[c] Laboratorio de Microscopías Avanzadas, Instituto de Nanociencia de Aragón, Universidad de Zaragoza, 50018 Zaragoza, Spain; Fundación ARAID, 50018 Zaragoza, Spain; and Fundación INA, 50018 Zaragoza, Spain.
[d] Instituto de Ciencia de Materiales de Aragón and Departamento de Física de la Materia Condensada, Universidad de Zaragoza, 50009 Zaragoza, Spain.
† Electronic Supplementary Information (ESI) available: [details of any supplementary information available should be included here]. See DOI: 10.1039/b000000x/
‡ Present address: Department of Biological Sciences, Columbia University, New York 10027
§ Present addres: Departamento de Física, Universidade de Lisboa, 1749-016 Lisboa, Portugal.

**Table 1** Free energy barrier height $\Delta G^{\dagger}$, position $x^{\dagger}$ and dissociation free energy $\Delta G^{0}$ for some biomolecular complexes. Typically $\Delta G^{0} > \Delta G^{\dagger}$ can be observed. (a), (b), (c) and (e) are presented in Refs.[27,29,22] and [24] respectively. (d) are obtained after an analysis of data given in [24] (seeSI). (f) is obtained in this work and (g) in [31].

| Complex | $\Delta G^{\dagger}[k_BT]$ | $x^{\dagger}$ [nm] | $\Delta G^{0}[k_BT]$ |
|---|---|---|---|
| Biotin:streptavidin | $13.6^{a}$ | $0.6^{a}$ | $30.9^{b}$ |
| Biotin:avidin | $11.7^{a}$ | $0.5^{a}$ | $33.7^{c}$ |
| LFA-1:ICAM1 | $8.6^{d}$ | $0.2^{d}$ | $15.5^{e}$ |
| LFA-2:ICAM2 | $7.6^{d}$ | $0.4^{d}$ | $14.3^{e}$ |
| FNR:Fld | $4.9^{f}$ | $0.6^{f}$ | $12.8^{g}$ |
| FNR:Fd | $6.9^{f}$ | $0.5^{f}$ | $13.5^{g}$ |

pulling apparatus, which retracts at constant rate $r_f$ until the complex dissociates at a certain rupture force. From this magnitude, one should be able to derive the main properties of the underlying free energy profile. We propose a simple analysis procedure which allows for recovering the relevant free energy magnitudes $\Delta G^{\dagger}$ and $\Delta G^{0}$ from rupture force measurements, by applying DFS theory [12,13,16,27,28] and Jarzysnki equality [18]. The method is applied to DFS-AFM experiments of the complexes formed by the flavoenzyme Ferredoxin-NADP$^{+}$ reductase (FNR) and its two protein partners Ferredoxin (Fd) and Flavodoxin (Fld) from cyanobacterium *Anabaena* PCC 7119. This system is paradigmatic for the study of the association mechanism of redox complexes, and their interaction mechanism has been carefully characterized [30–35].

We provide values for the barrier position $x^{\dagger}$ and height $\Delta G^{\dagger}$, and for the dissociation free energies $\Delta G^{0}$, which remarkably match the thermodynamic values determined in [31]. Different from the unfolding of biological macromolecules case, now the obtained equilibrium magnitude $\Delta G^{0}$ compares to that obtained from bulk experiments -such as calorimetry- since the initial (bound) and final (unbound) states are very similar.

In our analysis, a somehow surprising $\Delta G^{\dagger} < \Delta G^{0}$ is found. This result seems to be uniquitous in mechanical unbinding of compleses see Table 1, but does not suit the conventional picture of a molecular potential [36–38], pictured in Fig. 1A. Thus, the main objective of our work is to introduce a plausible model for the mechanical unbinding of biomolecular complexes that suits this observation. In this sense, and in order to provide a unified framework for understanding the physical properties of this process, we propose an alternative free energy profile, sketched in Fig. 1B. To study the validity of the proposed model and the consistency of our method, we perform stochastic numerical simulations and analyze them with the same procedure used with the experimental data. Thus, on the one hand we validate the use of a simple and robust analysis protocol in order to jointly determine $\Delta G^{\dagger}$ and $\Delta G^{0}$ from DFS experiments. On the other hand, we propose a free energy profile shape for mechanical dissociation of biomolecular complexes, focusing on the physical mechanism which drives this process. We finish with a thoroughly discussion on the biological implications of our results.

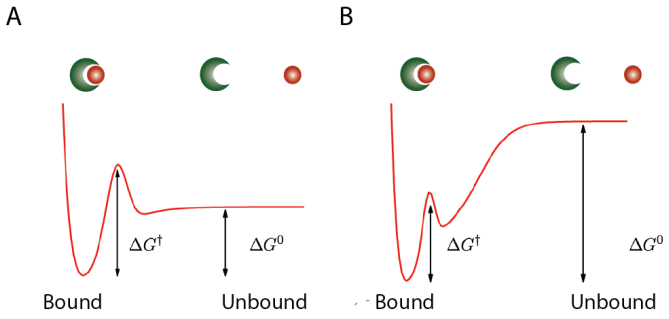


**Fig. 1** Free energy profile representation for the dissociation of biological complexes. The profile is characterized by a free energy barrier $\Delta G^{\dagger}$, and the dissociation free energy $\Delta G^{0}$. Panel (A) shows a conventional picture of an unbinding molecular potential, $\Delta G^{\dagger} > \Delta G^{0}$. Panel (B) shows our proposal, which meets the requirements found in DFS studies, $\Delta G^{\dagger} < \Delta G^{0}$.

## 2 Analysis Method

We describe the joint analysis protocol to extract the free energy magnitudes $\Delta G^{\dagger}$ and $\Delta G^{0}$ from DFS experiments. This protocol is applied both to experiments on two different protein:protein complexes and on stochastic simulation on a physical-based model (Fig. 2, panel A).

From each force-extension unbinding trajectory showing an unbinding event (see Fig. 2, panel B), the rupture force $f^{\dagger}$ is taken as the peak of the trace. Thus, a rate dependent rupture force histogram is generated. From dynamic force spectroscopy theory, we can obtain $\Delta G^{\dagger}$ and $x^{\dagger}$ from the dependence of the *most probable* rupture force on the loading rate as [16,27,39]:

$$f^{*} = \frac{\Delta G^{\dagger}}{\nu x^{\dagger}} \left[ 1 - \left( -\frac{k_B T}{\Delta G^{\dagger}} \log \frac{r_f x^{\dagger}}{\kappa k_B T} \right)^{\nu} \right] \qquad (1)$$

where $\nu$ is a parameter which depends on the analytical shape of the free energy profile (see below for further details and see Ref. [39] for a comment about the difference between the expression for the most probable and the mean rupture force). The zero force unbinding rate $k_0$ can be obtained from $\kappa$ and $\Delta G^{\dagger}$ as $k_0 = \kappa e^{-\Delta G^{\dagger}/k_B T}$.

As $\Delta G^{0}$ is an equilibrium magnitude, we can use Jarzynski equality [18] in order to infer it from non-equilibrium work measurements.

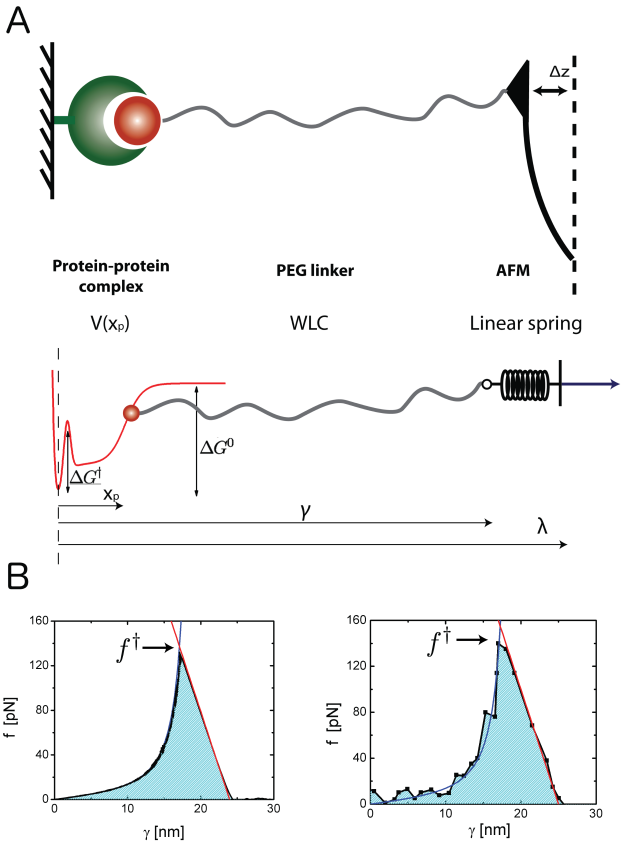


**Fig. 2 Panel (A)**: Graphical representation of the set-up for an unbinding force-spectroscopy experiment (upper) and scheme of the physical model (lower). The system is composed of two elements: first, the biological complex is modeled as a point particle moving in a phenomenological potential. Second, the pulling device (PEG polymer linker in series with the AFM cantilever) is modeled as a WLC model in series with a linear spring. There are three relevant coordinates, $x_p$ is the position of the particle in the potential, $\gamma$ the distance to the tip of the cantilever, while $\lambda$ is the control parameter such that $\lambda = Vt$. **Panel (B)**: Selected force extension curve for the simulated physical model (left) and experiment (right). Force on the spring is represented versus coordinate $\gamma$. Two clear regions can be identified. First, a WLC dependence of persistence length $P = 0.37nm$ and contour length $L_0 = 20nm$ is found (blue curve) up to the unbinding force $f$. Then, the force relaxes following a linear dependence of slope $K_C = 20pN/nm$. The area under the trace (shaded region) is the accumulated work upon the unbinding process (Eq. (4)).

$$e^{-\Delta G^0/k_BT} = \langle e^{-W/k_BT} \rangle, \tag{2}$$

where $\langle \cdots \rangle$ is the ensemble average over a fixed non equilibrium protocol. As we are subject to limited sampling, given a work distribution $P(W)$, we compute the Jarzynski estimator $\Delta G^0_J$. Considering a limited number $N$ of work measurements $W_i$, the Jarzynski estimator reads:

$$\Delta G^0_J = -k_BT \log \frac{1}{N} \sum_i^N e^{-W_i/k_BT}. \tag{3}$$

It is important to define correctly the non equilibrium protocol we use in order to compute the proper work distributions $p(W)$ [40]. Here, the work performed on the system is the integral of the rupture force with respect to the *control parameter* $\lambda$ (see Panel A at Fig. 2). In this regard, given a rupture trace $f(\lambda)$, the work is calculated as [41]:

$$W = \int_0^{\lambda^\dagger} f(\lambda) d\lambda = \int_0^{\gamma^\dagger} F_{WLC} d\gamma + \frac{1}{2} \frac{(f^\dagger)^2}{K_C}, \tag{4}$$

where $F_{WLC}$ is the force-extension curve of a WLC (see SI), $K_C$ the spring constant of the AFM cantilever and $\gamma$ and $\lambda$ are graphically defined in Fig. 2A. Equation (4) is equivalent to the work accumulated by the whole pulling device over the unbinding process (polymer linker and linear spring contributions). Jarzynski equality is exact, and thus independent of the pulling rate. Nevertheless, the exponential average leads to poor convergence, which is enhanced for slow rates. In this regard, we calculate the Jarzynski estimator $\Delta G^0_J$ as a function of the loading rate, expecting convergence to $\Delta G^0$ as the rate decreases.

## 3 Dynamic Force Spectroscopy Experiments

### 3.1 Methods

DFS measurements were carried out using the force spectroscopy mode in a Cervantes Fullmode SPM system (Nanotec Electrónica S.L, Spain). FNR molecules were labelled, separated and immobilized on mica surfaces, as described previously [42]. Maleimide-terminated flexible polyethylene glycol (PEG) linker silicon nitride AFM cantilevers with nominal spring constant of 20pN/nm (Novascan Technologies Inc, Ames, USA) were used. PEG polymer has a nominal stretched length of around $20nm$ (PEG MW 3400). $42\mu$M thiolated-Fld/Fd, labeled and purified as reported [35,42], were incubated on the maleimide-PEG-cantilevers in PBS, EDTA, pH 7.0 for 1 hour and washed extensively with the same buffer. Labelling and subsequent immobilization steps were performed to orient the interaction surfaces of both proteins one towards each other, which optimizes the recognition ability and the collection of successful unbinding events in DFS scans. A schematic view of the experimental set-up is depicted in Fig. 2 (upper).

Several hundred force-distance cycles were registered for Fd and Fld-cantilever/FNR-mica approaches at different loading rates, ranging from $2 - 80 \times 10^3$pN/s. Data were collected at a sampling rate of 16kHz, and subsequently averaged over 20 points. This sampling is suitable for obtaining $f^\dagger$ as explained in the text, see also Fig. 2(B). We use a PEG fingerprint to select the curves containing specific rupture events [24–26], which are characterized by a WLC-like increase in the force with the persistence and contour length of the polymer spacer (0.37nm and 20nm respectively) [43,44]. Furthermore, a careful orientation protocol was designed to increase the ratio of specific interactions, typically low. Although designed sophisticated fingerprints to distinguish specific forces have been reported [45,46], PEG marks were clear enough to select specific force events and those that offered doubts were dismissed. Additionally, negative control experiments were carried out by blocking the available FNR sites by incubating the samples with 0.70mM Fld. However, an unavoidable source of uncertainty in the experiment comes from small

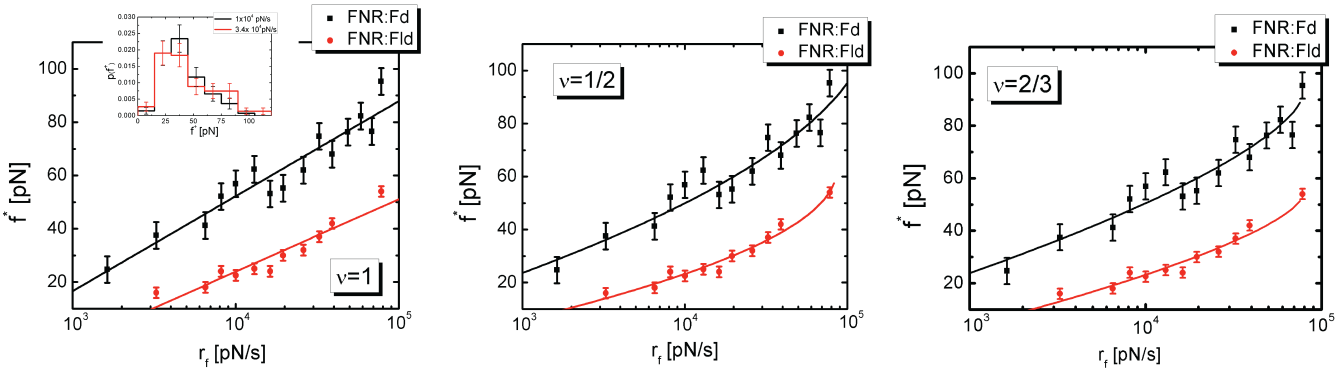


**Fig. 3** Typical rupture force $f^*$ as a function of the loading rate for the two protein:protein complexes, FNR:Fd (black) and FNR:Fld (red). The experimental data are fitted to Eq. (1) for the three models, $\nu = 1$ (Bell model, left panel), $\nu = 1/2$ (cusp-parabolic potential, central panel) and $\nu = 2/3$ (cubic potential, right panel). Parameters yielded for each case are shown in Table 2. Insets show the the rupture force distribution $P(f^\dagger)$ for two different loading rates $r_f$. $f^*$ is taken as the peak (mode) of the histograms.

**Table 2** Fitting parameters for Fig. 3 for the three different model exponents $\nu$. Intrinsic rate $k_0$, position of the transition state $x^\dagger$ and free energy barrier height $\Delta G^\dagger$ are provided but for Bell model $\nu = 1$. The quality of the fittings is evaluated with the reduced $\chi^2$ and $R^2$, as well as the Bayesian information criterion (BIC), see also SI.

| **Complex** | Model | $k_0$ | $\Delta G^\dagger$[k$_B$T] | $x^\dagger$ [nm] | $\chi^2/R^2$ | BIC |
|---|---|---|---|---|---|---|
| FNR:Fd | $\nu = 1$ | $0.044 \pm 0.016$ | – | $0.26 \pm 0.02$ | 1.32/0.90 | 42.3 |
| FNR:Fld | | $0.218 \pm 0.064$ | – | $0.34 \pm 0.04$ | 3.50/0.89 | 42.4 |
| FNR:Fd | $\nu = 1/2$ | $0.013 \pm 0.002$ | $7.69 \pm 0.71$ | $0.52 \pm 0.05$ | 1.28/0.91 | 43.4 |
| FNR:Fld | | $0.176 \pm 0.020$ | $5.43 \pm 0.44$ | $0.71 \pm 0.07$ | 1.33/0.96 | 32.8 |
| FNR:Fd | $\nu = 2/3$ | $0.018 \pm 0.002$ | $6.86 \pm 0.61$ | $0.46 \pm 0.02$ | 1.175/0.91 | 42.1 |
| FNR:Fld | | $0.110 \pm 0.022$ | $4.85 \pm 0.41$ | $0.56 \pm 0.01$ | 1.58/0.95 | 33.1 |

misalignment between the force at the attachment point and the unbinding direction coordinate. Further details on the experimental protocol can be found in the SI and [35,42].

Experiments are performed by moving the cantilever support at a constant velocity $V$. Loading rates are computed as $r_f = df/dt = K_{\text{eff}}V$ whith $K_{\text{eff}}$ the effective stiffness of the total, complex-linker-cantilever, system [47] $K_{\text{eff}}^{-1} = K_M^{-1} + K_L^{-1} + K_C^{-1}$. Usually $K_M \gg K_L, K_C$, and from the force-distance curves we estimate $K_L \simeq K_C$. Being $K_C = 20$pN/nm, it yields an effective stiffness $K_{\text{eff}} \simeq 10$ pN/nm (see SI for additional comments).

### 3.2 Results

We carry out DFS measurements of mechanical dissociation for the two different protein-protein complexes formed by the flavoenzyme Ferredoxin-NADP$^+$ reductase (FNR) and its two protein partners Ferredoxin (Fd) and Flavodoxin (Fld) from cyanobacterium *Anabaena* PCC 7119. Crystal structure of FNR:Fd complex is 1EWY while the FNR:Fld complex has not been crystalized. This system is paradigmatic for the study of the association mechanism of redox complexes, as two proteins of different nature (Fd and Fld) interact at the same binding site of FNR [30]. Additionally, they constitute a suitable system for our analysis proposal, as they share similar thermodynamic properties [31], while their interaction mechanisms are dissimilar, being that of Fd with FNR very specific, whereas that of Fld with FNR has low specificity, allowing multiple orientations on the FNR surface that are competent for the electron transfer process [32,48,49].

Each rate dependent force histograms $P(f^\dagger|r_f)$, see inset of Fig. 3, was built from typically $100-200$ specific events. From the experimental force histograms, the most probable rupture force $f^*$ is calculated as its mode. The showed histogram includes multievents which lead to long tails in the high force region. These events usually are not trivially identified. The analysis protocol we use is largely unaffected by them since we fit the typical rupture forces (not affected by high force tails), and we use the Jarzynski equality, which enhaces low force events, being the right tail events absolutely negligible.

Figure 3 shows the typical rupture force as a function of the loading rate $r_f$ for FNR:Fd (black) and FNR:Fld (red). As the actual barrier profile is uknown, we fit the data to Eq. (1) with three different exponents $\nu$, respectively Bell-Evans phenomenological model ($\nu = 1$,left panel) [13], a parabolic-cusp potential ($\nu = 1/2$, middle panel) [14] and a linear-cubic potential ($\nu = 2/3$, right panel) [16]. Table 2 shows the fitting parameters and the reduced $\chi^2$, the $R^2$ and the BIC values, in order to compare the quality of the fittings.

The fitting results show a difference between both complexes. For FNR:Fd the three models give similar selection criteria values. However, in the case of FNR:Fld both $\nu = 1/2$ and $\nu = 2/3$ yield significantly better fittings. Thus, from the point of view of the statistical analysis of the experimental data we can only discard the $\nu = 1$ model and for the FNR:Fld case.

From a physical point of view, fitting to the linear-cubic poten-

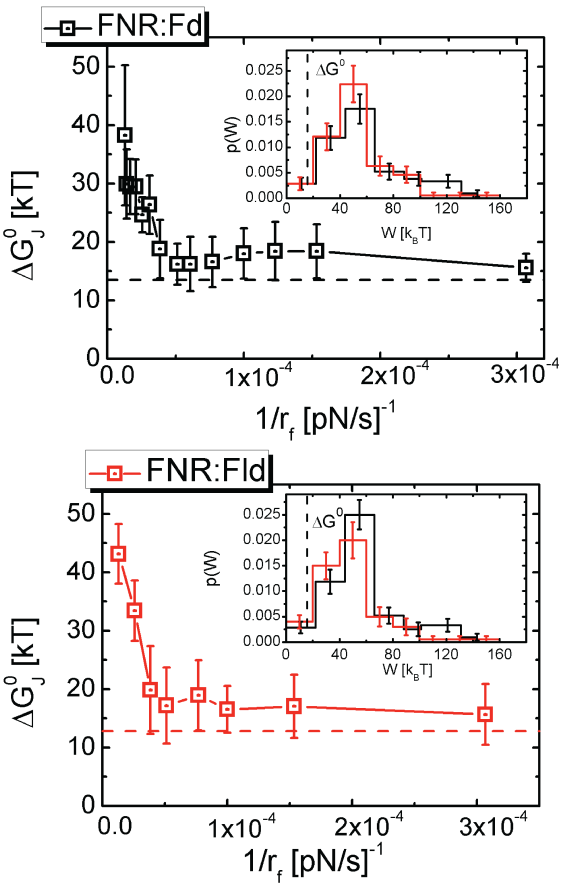


**Fig. 4** Evolution of the Jarzynski estimator $\Delta G^0_J$ with the inverse of the loading rate $1/r_f$ for the two analyzed protein-protein complexes FNR:Fd (left) and FNR:Fld (right). Error bars are calculated with Jackknife resampling method. The calorimetry-determined values for the dissociation free energy are marked by dashed lines, $\Delta G^0 = 13.49 k_B T$ for Fd-FNR and $\Delta G^0 = 12.82 k_B T$ for Fld-FNR. For high loading rates, a clear overestimation is observed with respect to $\Delta G^0$. Nevertheless, as the loading rate decreases convergence is achieved within error bars. *Inset*: Work distributions for two chosen loading rates with $\Delta G^0$ as a vertical dashed line.

tial likely gives the best estimation of the free energy parameters, as any analytical potential can be approximated by a cubic one when tilted by a force. We have seen that $\nu = 1/2$ and $\nu = 2/3$ yield good fittings, providing the height of the free energy barrier $\Delta G^\dagger$. Both fittings give similar free energy values which are in any case compatible with the discussion and conclusions of this work. Bell-Evans phenomenological model ($\nu = 1$) does not provide the curvature of the force dependence as observed at higher rates. Being the simplest theory, it does not account however for the shift of the transition state with the force, an effect which appears for most analytical potential shapes.

Each force distribution can be mapped onto the work distributions by means of Eq. (4). For each pulling rate, we calculate Jarzysnki estimator, by applying Eq. (3). Fig. 4 shows Jarzysnki estimator as a function of the inverse of the loading rate $1/r_f$, where the errors bars are calculated with Jackknife resampling method. Dashed lines indicate the dissociation free energy as obtained from calorimetric experiments[31] ($\Delta G^0_{Fd-FNR} = 13.5 \pm 0.2 k_B T$, $\Delta G^0_{Fld-FNR} = 12.8 \pm 0.2 k_B T$).

As already mentioned, a well known feature of Jarzynski estimator is its convergence behavior, which is readily illustrated in Fig. 4. At high loading rates (low values of $1/r_f$), the system is very far from equilibrium, and a non accesible number of experiments is needed (typically of the order of[50] $N \sim e^{(\langle W \rangle - \Delta G^0)}$). Nevertheless, for lower loading rates, here $r_f \sim 3 - 20 \times 10^3 pN/s$, the estimator converges to a fixed value, as the reduction of $\langle W \rangle$ allows $N$ to be of the order of $10^2$, the number of experiments used. Interestingly, the estimator converges to the calorimetric free energy, so the bias of the estimator indeed drops to zero. Several analytical effort has been put on developing expressions that would allow predicting the bias of Jarzynski estimator, and therefore improve the free energy estimation, when the system is far from equilibrium[51–53]. Such approaches are useful to improve convergence in the high pulling rate range, nevertheless they would make no difference in our free energy determination as we are able to measure in a pulling rate range where convergence is achieved. The application of the analytical correction to the Jarzynski estimator is shown in the SI.

## 4 Numerical simulations

### 4.1 Model

We propose and simulate a physical model for force-driven unbinding of biological complexes via force-spectroscopy experiments. Our model is made up of two main ingredients, according to the typical set-up used in these experiments. First, the biological complex is represented as a particle moving in a mesoscopic one-dimensional potential. Second, the pulling device is modeled as a Worm-Like Chain (WLC) model[43,44] representing the polymer linker -with $P$ the persistence length and $L_0$ the contour length- connected in series with a linear spring of stiffness $K_C$ modeling the AFM cantilever. This scheme is pictured in Panel A of Fig. 2.

In order to mimic the observed phenomenology, we characterize the free-energy profile by two magnitudes, the free energy barrier height $\Delta G^\dagger$ and the dissociation free energy $\Delta G^0$, such that $\Delta G^\dagger < \Delta G^0$. This condition is a key component observed in many experiments (see Table I), and will be further discussed. Mathematically, we choose (see S.I. for further information and detailed parameter set):

$$\begin{aligned} G(x_p) &= D(1 - e^{-a x_p})^2 + U e^{-(x_p - x^\dagger)^2/b} \\ &+ F_0 \left[1 + \tanh w(x_p - s)\right]. \end{aligned} \quad (5)$$

This profile reflects the three relevant regions in the unbinding process. The first term provides the equilibrium well at $x_p = 0$ which represents the bound state. The second term accounts for a brittle free energy barrier of height $\Delta G^\dagger \approx D + U$, width $b$ and placed at $x_p = x^\dagger$. The third term originates a smoother slope leading to the unbound state $\Delta G^0 = 2F_0 + D$, with characteristic length of $s/w$, distance over which the complex dissociates. The exact analytical expression of the potential is not decisive for the model success, providing it exhibits a first brittle slope of height

$\Delta G^{\dagger}$ and the second smooth slope leading to the unbound state $\Delta G^0$.

This particle is subject to a force exerted by the pulling device, as the end of the linear spring moves at a constant velocity $V$, so that its position is a controlled parameter $\lambda = Vt$. As in the experimental case, the loading rate is defined as $r_f = df/dt = K_{\text{eff}}V$ with $K_{\text{eff}} \simeq 10$ pN/nm. In order to simulate rupture trajectories, we integrate the Langevin equation of motion (see SI):

$$m\ddot{x}_p = -\eta\dot{x}_p - \nabla G(x_p) + F_{WLC}(\gamma - x_p) + \xi(t), \qquad (6)$$

being $m$ the mass of the particle, $\eta$ the viscous damping, $\xi(t)$ the thermal white noise, and $\gamma$ the distance from the origin to the end of the polymer, so that $\gamma - x_p$ is the polymer extension (see Fig. 2). Thus, $F_{WLC}(\gamma - x_p)$ is the force exerted by the polymer, which equals that of the linear spring, $F_{WLC} = K_C(\gamma - Vt)$.

### 4.2 Results

We have simulated the Langevin equation of the system. We set the profile parameters such that $\Delta G^{\dagger} = 7.7 k_B T$, $\Delta G^0 = 14.7 k_B T$ and $x^{\dagger} = 0.5$nm, values close to those found in the experimental studies of the system. The loading rates range was chosen so that the most probable rupture forces span over the experimental range ($f^* \sim 20 - 100pN$). For each simulated rate, we ran $10^4$ realizations, saving the rupture force $f^{\dagger}$ for each trajectory. The most probable rupture force $f^*$ is calculated as the maximum of the force histogram. Force histograms are then mapped into work histograms using Eq. (4).

Figure 5 (top) shows the most probable unbinding force as a function of the loading rate. Fitting to Eq. (1) with $\nu = 2/3$, we obtain $\Delta G^{\dagger} = 7.28 \pm 0.20 k_B T$, $x^{\dagger} = 0.35 \pm 0.08 nm$, $\kappa = 5.44 t^{-1}$ -time units defined in SI-, matching the values set in the free energy profile. As shown, the agreement between the simulated data and the fitting protocol is excellent. A comparison with the fitting to the $\nu = 1/2$ case is given in the SI. The $\nu = 1$ model is unable to reproduce the curvature of the data at high pulling rates. Equation (1) was derived for a particle pulled by a soft linear spring and hopping over an energy potential, which is a good approximation in most cases, proving it to be a suitable tool for analyzing this kind of processes.

Figure 2 might suggest that unbinding occurs surmounting two potential barriers, a situation where Eq. (1) is not valid. However this second barrier, with a smaller slope, disappears at small forces. At typical rupture forces a single barrier profile is obtained. Nevertheless, rare events exist, where the system escapes thermally for low pulling forces, jumping over the two barriers. Such events can be observed as the small shoulder which appears at low forces $f \sim 20pN$ in the distributions $P(f^{\dagger})$ (see inset on Fig. 5 top), which do not affect the $f^*$ determination.

In Fig. 5 (bottom) we plot the Jarzynski estimator $\Delta G_J^0$ as a function of the inverse of the loading rate, where the error bars are calculated with Jackknife resampling method. The blue solid line indicates the unbinding free energy $\Delta G^0 = 14.7 k_B T$. Clearly the estimator converges to this value as we decrease the pulling rate. Nevertheless, it must be noted that the convergence is far faster than that seen in the experimental system, as we are averaging over $10^4$ realizations, compared to the $\sim 10^2$ experimental curves used.

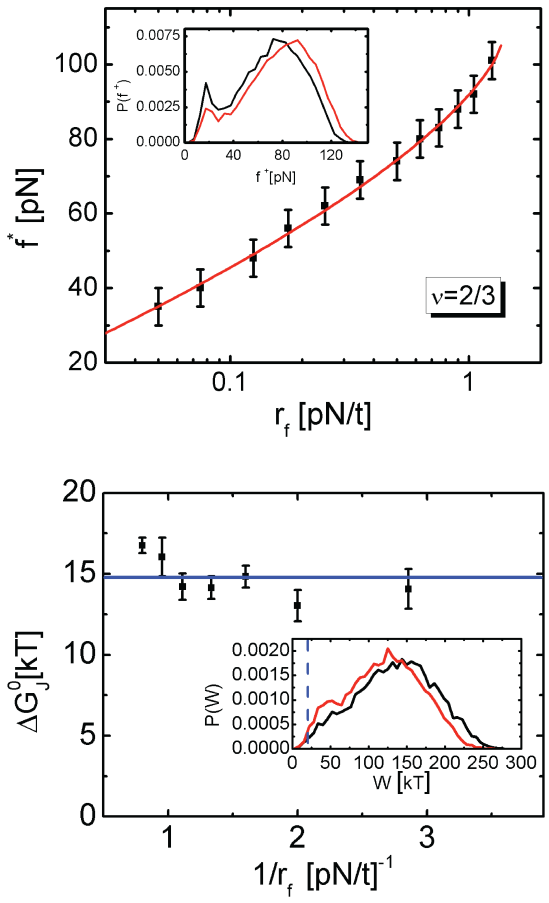


**Fig. 5** *Top*: Typical rupture force $f^*$ as a function of the loading rate $r_f$ in semi-logarithmic scale, simulated for potential Eq. (5) with parameters set such that $\Delta G^{\dagger} = 7.7 k_B T$ and $x^{\dagger} = 0.5nm$. Fitting to Eq. (1) yields $\Delta G^{\dagger} = 7.28 \pm 0.2 k_B T$, $x^{\dagger} = 0.35 \pm 0.08 nm$ and $\kappa = 5.44 t^{-1}$. *Inset*: Distribution of rupture forces for two selected rates. *Bottom*: Evolution of the Jarzynski estimator $\Delta G_J^0$ as a function of the inverse of the loading rate $1/r_f$ simulated for potential Eq. (5), with parameters such that $\Delta G^0 = 14.7 k_B T$, indicated with solid blue line. Clear convergence is observed, especially for lower loading rates. *Inset* Work distributions for two selected rates, with $\Delta G^0$ as a dashed line.

In the inset, we show the $P(W)$ for two chosen loading rates, with a vertical dashed line at $\Delta G^0$. Quasistatic pulling would lead to $P(W) = \delta(W - \Delta G^0)$, where $\delta(x)$ is the Dirac delta distribution. As we are pulling out of equilibrium, $\langle W \rangle > \Delta G^0$, but for some rare events we obtain $W < \Delta G^0$ which allows the Jarzynski estimator to converge. This fact is consistent with previous commentary, as these low work rare events arise from low force escapes, where the particle actually "sees" the smooth barrier which leads to the unbound state.

## 5 Discussion

In this work we have shown that, by employing a suitable analysis protocol, DFS experiments can be used to obtain both the kinetic and thermodynamic properties of ligand:receptor com-

plexes. Our analysis method lies on the free energy profile we introduce to model the unbinding process. The shape of this profile is motivated by an apparent paradox we find in many ligand:receptor complexes, where $\Delta G^{\dagger} < \Delta G^{0}$. This condition appears to be ubiquitous for mechanical unbinding of biological complexes, as shown in Table I where results of different works are collected.

The main characteristic of the proposed free energy profile is the scale separation between a short range steep barrier, and the second smooth slope. In DFS experiments, the bias exerted by the pulling force tilts the profile with a $-fx_p$ term, see Panel A in Fig. 6. The second smooth slope vanishes at small pulling forces, and the system escapes *on average* through a single barrier profile. With low probability, the system will reach the unbound region at very low force, and this rare escape will carry information about the second region which has not vanished yet, contributing to the low force tail. By taking advantage of this uncoupling between $\Delta G^{\dagger}$ and $\Delta G^{0}$, we obtain both magnitudes by a joint application of force spectroscopy theory and Jarzysnki equality. While Eq. (1) accounts for the typical or average contributions, Jarzysnki equality, due to exponential averaging, enhances low force tails.

This two uncoupled regions are also motivated by the physical process of unbinding, corresponding to different physical situations, see Panel B in Fig. 6. The first region reflects the local short-ranged molecular interactions between the interface residues which keep the complex in the bound state. This is modeled effectively by a steep free energy barrier located within few Å. Over the barrier, first water molecules would enter the intermolecular region, solvating partially the interacting surfaces, and thus lowering the profile. The second region should account for the complete dissociation between both molecules and thus span over few nanometers. This interaction region is originated by long-range non-specific interactions, likely originated by the coupling between the dipolar moments of the molecule. This is modeled as the smooth slope which leads to the plateau where the interaction vanishes. In this regard both analysis methods are insensitive to minor details of the specific landscape in the coupling region since DFS probes the barrier and Jarzynski the unbinding energy.

We applied our analysis method on AFM experiments for two protein:protein complexes, and on stochastic simulations on a physical-based model. While the experimental results yielded valuable information about the physical properties of the studied systems, the numerical simulations helped in validating the protocol, as they successfully recovered the magnitudes set in the profile at zero force. A relevant advantage of our procedure it is its robustness, as the only necessary output from the experiments is the rupture force, allowing for a systematic application and interpretation of the results. Nevertheless, a faithful analysis requires to measure a considerable number of specific unbinding events, making it necessary to adopt functionalization strategies, as random targeting suffers of low efficiency in bond formation. In our case, the immobilization strategy used to orient both the interaction surface of FNR and protein ligands towards each other on mica and AFM tips, respectively, allowed us to achieve a high efficiency in getting successful specific rupture events[35,42].

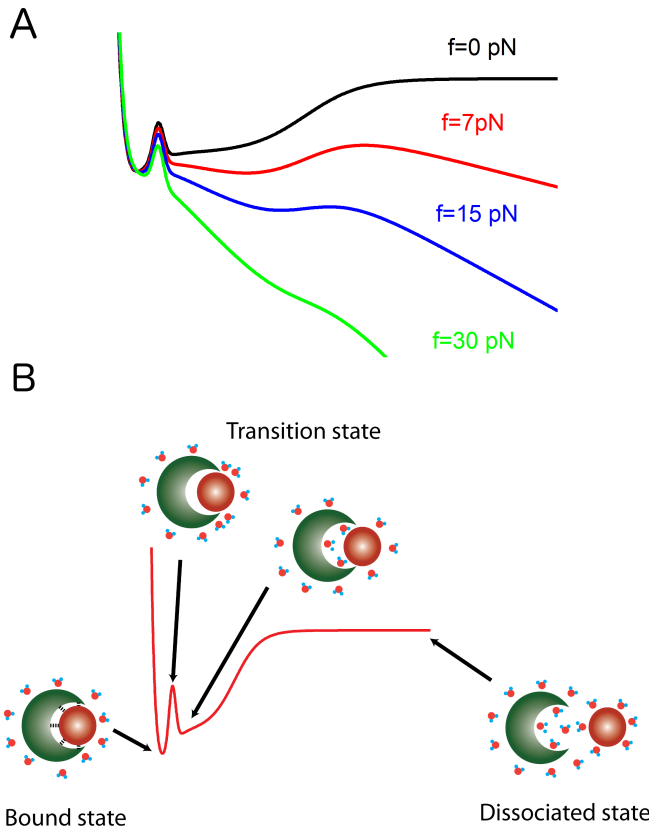


**Fig. 6 Panel (A)**: Free Energy profile tilted for different values of the pulling force. At very small forces $(5-10pN)$, the smooth region survives and the system escapes surmounting two effective barriers. When the force rises, the profile is completely equivalent to a single-barrier profile, and the second barrier is not seen by the system. **Panel (B)**: Schematic view for the physical interpretation of the proposed free energy profile for mechanical dissociation of biological complexes. We can distinguish different interaction regions upon the mechanical dissociation process. First the steep inner barrier must be overcome, involving the rupture of the short-range molecular bonds between the interacting surfaces. Then, the first water molecules access the interface region decreasing, the free energy of the system. In order to dissociate completely the complex, the molecules must be separated within few nanometers solvating completely the intermolecular space and overcoming the electrostatic interaction due to the dipolar moment coupling of the two proteins.

Protein:protein complexes are of particular interest. Particularly the studied system composes a singular case, as Fd and Fld are common binding partners of FNR using the same interaction surface on the flavoenzyme, as undoubtedly verified[30,31,34]. FNR catalyzes the transfer of two electrons to reduce $NADP^{+}$ to NADPH from two independent Fd molecules, while in some algae and cyanobacteria, Fld replaces Fd under iron-deficient conditions[31,32]. While both share similar binding affinities[31], they are known to display different interaction mechanisms[31,33,34,48,49]. It is demonstrated that Fd binding is more specific, and forms an only complex maintained mainly through specific electrostatic interactions. Nevertheless, it has not been found any key residue for Fld binding, contrary to Fd, and different orientations between Fd and FNR are equally efficient for electron transfer. The fact that crystallization of the FNR:Fld complex has not been achieved is

also indicative of this. The size of the interacting surfaces are different, the binding site for Fld is smaller, which shows a lower variation of the $C_p$ value on binding, and the release of 20 water molecules per 30 for Fd binding to FNR[31].

Our findings from the analysis of DFS experiments match previous knowledge on the energetics of these complexes, providing in addition novel information, particularly about their kinetic behavior. On the one hand, we recover the thermodynamic features of both complexes, reflected in moderate affinities which are very similar in both cases ($\Delta G^0 \approx 13 k_B T$). The unbinding free energies calculated through Jarzysnki equality agree respectively within error bars with the calorimetric binding free energy reported in[31]. In any case, a small difference could be expected due to the presence of a tether linked to the ligand, which increases the free energy of the unbound state relative to the equilibrium (tether-free) unbound state.

Nevertheless, despite these similar equilibrium characteristics, we found significant differences in their kinetic behaviors, as the obtained free energy barriers heights contrast considerably ($\Delta G^\dagger \approx 7 k_B T$ for FNR:Fd and $\Delta G^\dagger \approx 5 k_B T$ for FNR:Fld). These differences might be attributed to the particular features concerning the formation of each complex. Showing a larger interacting interface, Fd binding to FNR is more specific, with salt bridges between certain key positive residues on the FNR surface and acidic residues on Fd[32,48,49,54], which would contribute in addition to other non-specific interactions such as hydrogen bonds or the hydrophobic effect. On the contrary, kinetic analysis of side-directed mutants and docking studies on FNR:Fld suggest that Fld can adopt multiple orientations on the FNR surface, and that charged residues are not involved in crucial specific interactions[32,33,48]. In this sense, this features agree with our findings. Upon complex rupture, specific short range-interactions contribute decisively to the FNR:Fd interaction, reflected in a higher free energy barrier when compared to FNR:Fld, whose binding mechanism is mainly due to the hydrophobic effect.

To conclude, we have presented a simple and consistent analysis method for force-induced dissociation experiments in different biological complexes (protein:protein, protein:ligand or enzyme:substrate for instance). The method relies on a novel free energy profile we introduce to model this process. Our proposed method and model is of general application to any biological problem of interest which involves mechanical dissociation of complexes. In addition, different from the case of mechanical stretching, in mechanical unbinding problems the obtained dissociation free energy can be directly compared with the thermodynamic binding energy. In this sense, our work bridges the gap between single-molecule and bulk experiments.

## Acknowledgements

The authors thank M. Medina and A. Velázquez-Campoy for useful discussions and J. L. Díez and I. Echániz for technical support. The authors thank specially also J. Alegre-Cebollada, for useful commentaries and improvements in the manuscript version. The authors acknowledge support from the Spanish MINECO, project FIS2011-25167, FIS2014-55867, BIO2013-42978-P and MAT2012-38318, and Departamento de Industria e Innovación of Gobierno de Aragón and Fondo Social Europeo (FENOL and Biología Estructural group). A.L. thanks ARAID for financial support. R.T. thanks Spanish MECD for receiving a predoctoral fellowship. C.M. is indebted to Gobierno de Aragón for receiving a predoctoral fellowship.

## References

1 Bhutan, B., Ed.; In *Scanning Probe Microscopy in Nanoscience and Nanotechnology.* Springer-Verlag, 2012;
2 Borgia, A.; Williams, P.; Clarke, J. *Annu. Rev. Biochem.* **2008**, *77*, 101.
3 Bustamante, C.; Chemla, Y. R.; Forde, N. R.; Izhaky, D. *Annu. Rev. Biochem.* **2004**, *73*, 705.
4 Neumann, K. C.; Nagy, A. *Nat. Methods.* **2008**, *5*, 491.
5 Puchner, E. N.; Gaub, H. E. *Curr. Opin. Struct. Biol.* **2009**, *19*, 605.
6 Williams, M. C.; Rouzina, I. *Curr. Opin. Struct. Biol.* **2002**, *12*, 330.
7 Florin, E. L.; Moy, V. T.; Gaub, H. E. *Science* **1994**, *264*, 415.
8 Rief, M.; Gautel, M.; Oesterhelt, F.; Fernández, J.M.; Glaub, H. E. *Science* **1997**, *276*, 1109.
9 Liphart, J.; Onoa, B.; Smith, S. B.; Tinoco, I.; Bustamante, C. *Science* **2001**, *292*, 733.
10 Merkel, R.; Nassoy, P.; Leung, A.; Ritchie, K.; Evans, E. *Nature* **1999**, *397*, 50.
11 Alegre-Cebollada, J.; Perez-Jimenez, R.; Kosuri, P.; Fernandez, J. M. *J. Biol. Chem.* **2010**, *285*, 18961.
12 Garg, A. *Phys. Rev. B* **1995**, **51**, 15592.
13 Evans, E.; Ritchie, K. *Biophys. J.* **1997**, *72*, 1541.
14 Hummer, G.; Szabo, A. *Biophys. J.* **2003**, *85*, 5.
15 Dudko, O. K.; Filippoc, A. E.; Klafter, J.; Urbakh, M. *Proc. Natl. Acad. Sci. USA* **2003**, *100*, 11378.
16 Dudko, O. K.; Hummer, G.; Szabo, A. *Phys. Rev. Lett.* **2006**, *96*, 108101.
17 Mazo, J.J.; Fajardo, O.Y.; Zueco, D. *J. Chem. Phys.* **2013**, *138*, 104105.
18 Jarzysnki, C. *Phys. Rev. Lett.* **1997**, *78*, 2690.
19 Liphardt, J.; Dumont, S.; Smith, S. B.; Tinoco, Jr. I.; Bustamante, C. J. *Science* **2002**, *296*, 1832.
20 Hummer, G.; Szabo, A. *Proc. Natl. Acad. Sci. USA* **2000**, *98*, 3658.
21 Alemany, A.; Mossa, A.; Junier, I.; Ritort, F. *Nature Phys.* **2012**, *8*, 688.
22 Green, N. M. *Adv. Protein Chem.* **1975**, *29*, 1.
23 Zhang, X.; Bogorin, D. F.; Moy, V. T. *Chem. Phys. Chem.* **2004**, *5*, 175.
24 Wojcikiewicz, E. P.; Abdulreda, M.H.; Zhang, X.; Moy, V. T. *Biomacromolecules* **2006**, *7*, 3188.
25 Bizzarri, A. R.; Cannistraro, S. *J. Phys. Chem. B* **2009**, *113*, 16449.
26 Bizzarri, A. R.; Cannistraro, S. *Phys. Chem. Chem. Phys.* **2009**, *13*, 2733.
27 Hyeon, C.; Thirumalai, D. *J. Chem. Phys.* **2012**, *137*, 055103.

28 Hänggi, P.; Talkner, P.; Borkovec, M. *Rev. Mod. Phys.* **1990**, *62*, 251.

29 Weber, P. C.; Wendoloski, J. J.; Pantoliano, M. W.; Salemme, F. R. *J. Am. Chem. Soc.* **1992**, *114*, 3197.

30 Martínez-Júlvez, M.; Medina, M.; Gómez-Moreno, C. *J. Biol. Inorg. Chem.* **1999**, *4*, 568.

31 Martínez-Júlvez, M.; Medina, M.; Velázquez-Campoy, A. *Biophys. J.* **2009**, *96*, 4966.

32 Medina, M. *FEBS Journal* **2009**, *276*, 3942.

33 Medina, M.; Abagyan, R.; Gómez-Moreno, C.; Fernández-Recio, J. *Proteins* **2008**, *72*, 848.

34 Medina, M.; Gómez-Moreno, C. *Photosynth. Res.* **2004**, *79*, 113.

35 Marcuello, C.; de Miguel, R.; Martínez-Julvez, M.; Gómez-Moreno, C.; Lostao, A. *Chem. Phys. Chem.* **2015**, 16, 3161.

36 Noy, A.; Friddle, R. W. *Methods* **2013**, *60*, 142.

37 Friddle, R. W.; Noy, A.; De Yoreo, J. J.; *Proc Natl Acad Sci USA*. **2012**, *34*, 135173.

38 Pierse, C. A.; Dudko, O. *Biophys. J.* **2013**, *105*, L19.

39 An approximate expression for the *mean* rupture force can be used introducing a $e^{-\widetilde{\gamma}}$ factor in the argument of the logarithm function in Eq. (1), where $\widetilde{\gamma}$ is the Euler-Mascheroni constant $\widetilde{\gamma} = 0.577....$

40 Mossa, A.; de Lorenzo, S.; Huguet, J. M.; Ritort, F. *J. Chem. Phys.* **2009**, *130*, 234116.

41 In this definition we are neglecting angle deviations in the pulling of the molecular complex which introduce a small error, in general difficult to account. See Ribezzi-Crivellari, M., Ritort F. *Biophys. J* **2012**, *103*, 1919.

42 Marcuello, C.; de Miguel, R.; Gómez-Moreno, C.; Martínez-Júlvez, M.; Lostao, A. *Protein Eng. Des. Sel.* **2012**, *25*, 715.

43 Marko, J. F.; Siggia, E. D. *Macromolecules* **1995**, *28*, 8759.

44 Bouchiat, C.; Wang, M. D.; Allemand, J.; Strick, T.; Block, S. M.; Croquette, V. *Biophys. J.* **1999**, *76*, 409.

45 Stahl,S. W.; Nash,M. A,; Fried, D. F.; Slutzki, M.; Barak, Y.; Bayer, E. A., Gaub H. E., *Proc. Natl. Acad. Sci. USA* **2012**, 109, 2043.

46 Schoeler, C.; Malinowska, K.H.; Bernardi, R. C.; Milles, L. F.; Jobst, M. A.; Durner, E.; Ott, W.; Fried, D. B.; Bayer, E. A.; Schulten, K.; Gaub, H.E.; Nash, M. A. *Nat. Comm.* **2014**, 5, 5636.

47 Alemany, A.; Rey-Serra, B.; Frutos, S.; Cecconi, C.; Ritort F. *Biophysical Journal* **2016**, 110, 63.

48 Goñi, G.; Herguedas, B.; Hervás, M.; Peregrina, J. R.; De la Rosa, M. A.; Gómez-Moreno, C.; Navarro, J. A.; Hermoso, J. A.; Martínez-Júlvez, M.; Medina, M. *Biochim. Biophys. Acta* **2008**, *1787*, 144.

49 Goñi, G.; Serrano, A.; Frago, S.; Hervás, M.; Peregrina, J. R.; De la Rosa, M. A.; Gómez-Moreno, C.; Navarro, J. A.; Medina, M. *Biochemistry* **2008**, *47*, 1207.

50 Jarzynski C. *Phys. Rev. E.* **2006**, *73*, 046105.

51 Palassini M.; Ritort F. *Phys. Rev. Lett.* **2011**, *107*, 060601.

52 Zuckerman D. M.; Woolf T. B. *Phys. Rev. Lett.* **2002**, *89*, 180602

53 Gore J.; Ritort F.; Bustamante C. *Proc. Natl. Acad. Sci. U.S.A.* **2003**, *100*, 12564

54 Morales, R.; Charon, M. H.; Kachalova, G.; Serre, L.; Medina, M.; Gómez-Moreno, C.; Frey, M. *EMBO reports* **2000**, *1*, 271.

# SUPPLEMENTARY INFORMATION: Physical Picture for Mechanical Dissociation of Biological Complexes: from Forces to Free Energies

R. Tapia-Rojo, C. Marcuello, A. Lostao, C. Gómez-Moreno, J.J. Mazo and F. Falo

# 1 Force espectroscopy experiments

*Functionalization.* The typical random immobilization on AFM tips and samples leads to many of the immobilized protein molecules are unable to interact with their partners because their interacting surfaces are used to anchor them to the support, which makes binding and subsequent rupture only occurring in a small percentage of approaches. Herein, an implemented procedure for tip and sample functionalization optimizing the recognition ability was used. Each protein molecule has a few lysine residues in their structure. First, once the protein complexes were formed, Sulfo-LC-SPDP crosslinker bound randomly to the primary amino groups of superficial lysines, and then labeled proteins were separated chromatographically from each FNR complex. Later, proteins were reduced with DTT and left exposed reactive sulfhydryl groups reacted with maleimide-PEG tips, forming disulfide bonds, or reacted with the thiol protected PDP groups in the case of the mica substrates. Thus, both partners were immobilized exposing the interaction surface of one molecule towards the other [Ref. 41 in the ms].

This method achieved a large increase in successful rupture events with respect to the corresponding random labeling using the same procedure, as was analyzed previously in detail [Ref. 34 in the ms]. The results range from 5-23%, with random labeling, to 40-77% with Fld-tagged tips and 34-61% for Fd-tagged probes in efficiency ratio for "useable curves" showing specific unbinding events regarding the total approaches. The increase with regard the randomly functionalized samples oscillated between 3-13 and 2-4 times for Fld and Fd approaches, respectively, and the differences attributed to the type of complex [Ref. 34 in the ms].

*Selection of the specific forces.* The total adhesion peaks generated during each force-distance curve either originates from a specific interaction (formation of a FNR-Fd/Fld bond) or from a non-specific one of any other origin. The use of PEG spacers to attach protein ligands to the AFM tip in unbinding DFS studies increase the length and flexibility of the sensor, allowing the molecules to freely move favoring first recognition and later the identification of the specific forces at the scans. The feature-rich stretching profile in water presented by PEG tethers constitutes

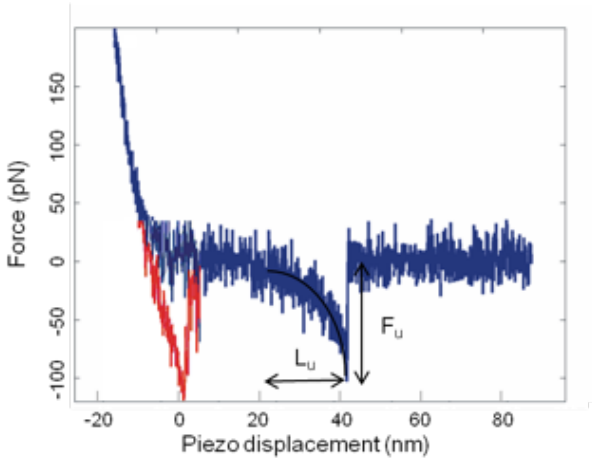


Figure 1: Representative experimental retraction force curve for a specific unbinding event corresponding to a single FNR-Fd complex. The Fz scan shows also a non-specific adhesion peak -in red to be distinguished- that follows the slope of the retraction. The unbinding event occurs at the unbinding length or tip-sample separation that is close to the length of the linker, around 20 nm, given by the piezo displacement encompassing the non-linear portion of the retraction curve before the rupture. The black line at this part represents the corresponding stretch of PEG according the WLC function. The shape of the force peak and the distance at which occurs ensure specificity. These considerations add certainty that measured rupture forces come from recognition events under study and not from artifacts or non-specific tip-sample adhesions.

a fingerprint of specificity, so specific force peaks show a nonlinear delay parabolic-like shape, which is characteristic of the stretching of a PEG linker, preceding the jump. The flexible tether sustains the increasing force until the complex dissociates, as indicated by a sudden jump to zero force. This occurs at a certain force value (unbinding force, $F_U$) and tip-sample distance (unbinding length, $L_U$). In contrast, in non-specific adhesions the contact curve extends towards negative values keeping the same slope, indicating that the bare tip, not the sensor, remains in contact with the surface. Figure 1 shows a representative Fz curve describing the two adhesion types. Control experiments were developed adding an excess of free ligand to block the FNR binding sites, at different R and for both type of complexes. In all the cases, they produced an important decrease in successful rupture events, giving very similar more probable rupture forces at the histograms, thus verifying the specificity and correctness of the measurements [Ref. 34 in the ms].

## 2 Potential Model and Simulation Details

We model the free energy profile for a mechanical rupture of a biological complex event as:

$$G(x_p) = D(1 - e^{-ax_p})^2 + Ue^{-(x_p - x^\dagger)^2/b} + F_0\left[1 + \tanh w(x_p - s)\right]. \tag{1}$$

Each one of the three terms of this profile reflects one of the three characteristic regions of this system: 1) a Morse potential creating an equilibrium well for the bound state; 2) a Gaussian barrier for the first steep barrier; 3) a tanh term for the smooth slope to the dissociation state, as an energetic plateau. In this sense, we can relate the free energy magnitudes with the parameters of the potential $\Delta G^\dagger \approx D+U$ and $\Delta G^0 = D+2F_0$. The remaining parameters set the qualitative shape of the profile, set such that the we have a steep first slope and a smooth second slope.

The exact set of parameters is : $D = 12$pNnm, $a = 3\text{nm}^{-1}$, $U = 24$pNnm, $x^\dagger = 0.5$nm, $b = 0.03\text{nm}^{-2}$, $F_0 = 24$pNnm, $w = 0.75\text{nm}^{-1}$ and $s = 4.0$nm, setting a free energy barrier $\Delta G^\dagger = 7.7k_BT$ and $\Delta G^0 = 14.7k_BT$.

We want to stress that the exact shape of this profile is not a critical aspect of the model, as long as we maintain the scale separation of the two slopes.

## 3 Simulation protocol

Numerical force spectroscopy experiment simulations are carried out by integrating the Langevin equation of motion,

$$m\ddot{x_p} = -m\eta\dot{x_p} - \nabla G(x_p) + F_{WLC}(\gamma - x_p) + \xi(t), \tag{2}$$

where $m$ is the reduced mass of the complex, $\eta$ the viscous damping and $\xi(t)$ white thermal noise. The term $-\nabla G(x_p)$ is the force derived from the movement in the free energy profile, while $F_{WLC}$ is the force exerted by the polymer, modeled, by a Worm Like Chain model:

$$F_{WLC}(x) = \frac{k_BT}{P}\left[\frac{1}{4}\left(1 - \frac{x}{L}\right)^{-2} - \frac{1}{4} + \frac{x}{L}\right], \tag{3}$$

where $P$ is the persistence length, $P = 0.37nm$ for the PEG polymer used here, and $L$ its contour length ($L = 20nm$ in our case).

Regarding the involved coordinates, $x_p$ is the coordinate of the particle moving in the free energy profile $G(x_p)$ while $\gamma$ is the distance of this particle to the linear spring (AFM tip), such that $\gamma - x_p$ is the extension of the WLC linker (polymer linker), and thus $F_{WLC}(\gamma - x_p)$ is the

force exerted by the polymer. As the AFM moves at constant velocity (force-extension mode), $\lambda = Vt$ is a control parameter (not fluctuating), which can be expressed as $\lambda = \gamma + F_{WLC}/K_c$, being $K_c$ the elastic constant of the linear spring. Here we consider that force equilibrium at the tip of the AFM, and thust $F_{WLC}(\gamma - x_p) = K_c \Delta z$, where $\Delta z$ is the elongation of the linear spring. This is a reasonable assumption due to the scale separation between the AFM tip ($\sim \mu m$) and the polymer linker ($\sim nm$).

The Langevin equation of motion is integrated by a fourth-order Runge-Kutta stochastic algorithm. Choosing a certain pulling velocity $V = \lambda/t$, we run numerical experiments starting at $\lambda = 0$ and stopping at $\lambda = 40nm$ to ensure that the rupture event has taken place (polymer length is $L = 20nm$). This is looped for 10000 realizations for each pulling velocity.

We use normalized time and mass units $\tilde{m} = 1$ and $\tilde{t} = 1$, but $pN$ units for force and $nm$ for length, given that we are mainly interested in comparing forces, lengths and energy with the experiments. Simulations are carried out at room temperature $T = 4.1pNnm = k_B T$. The damping in the normalized time units is $\eta = 10$.

# 4 Calculation of the work performed over a force-extension trajectory

As discussed in [1], the proper definition for the non-equilibrium work performed on a system is $dW = Fd\lambda$, where $\lambda$ is a control parameter (in contrast with fluctuating variables, which are stochastic variables) Here $d\lambda = Vdt$- where $V$ is the pulling velocity of the cantilever. According to Fig. 1 in main text, $\lambda = \gamma + \Delta z$, where $\Delta z$ is the cantilever deflection, modeled as a linear spring, so $\Delta z = F/K_C$. The work accumulated along a non-equilibrium transition from $\lambda = 0$ to $\lambda^\dagger$, where $\lambda^\dagger$ is a sufficiently large value of $\lambda$ so that the rupture event has occurred[1], is defined as:

$$W = \int_0^{\lambda^\dagger} F(\lambda) d\lambda. \tag{4}$$

By changing the variable to $\gamma$ (and neglecting the change in the coordinate $x_p$), we obtain

$$W = \int_0^{\gamma^\dagger} F_{WLC} d\gamma + \frac{1}{2}\frac{f^\dagger}{K_C}. \tag{5}$$

In this sense $W$ depends only on the rupture force $f^\dagger$.

# 5 Fitting of experimental data from other complexes

Table I in main manuscript shows data for $\Delta G^\dagger$ and $\Delta G^0$ for six different ligand-receptor complexes, including the FNR-Fd and FNR-Fld analyzed here, showing how $\Delta G^0 > \Delta G^\dagger$ is found. $\Delta G^0$ values are taken from calorimetry experiments. $\Delta G^\dagger$ are determined from force spectroscopy measurements. In order to determine them we reinterpret the original data in the context of our model.

Dynamic force spectroscopy AFM experiments for LFA-1:ICAM-1 and LFA-1:ICAM-2 complexes expressed in Jurkat cells where originally published in [2], and interpreted within a two-barrier profile obtaining by a two-region fitting of Bell-Evans expression. As discussed in the

[1] In the case of mechanical unbinding the exact value of $\lambda^\dagger$ is not critical, as once the rupture event has occurred, the interaction disappears and thus $\langle F \rangle = 0$ from then on. This is different from stretching of biomolecules where, once denatured, and underlying polymer stretching is still present

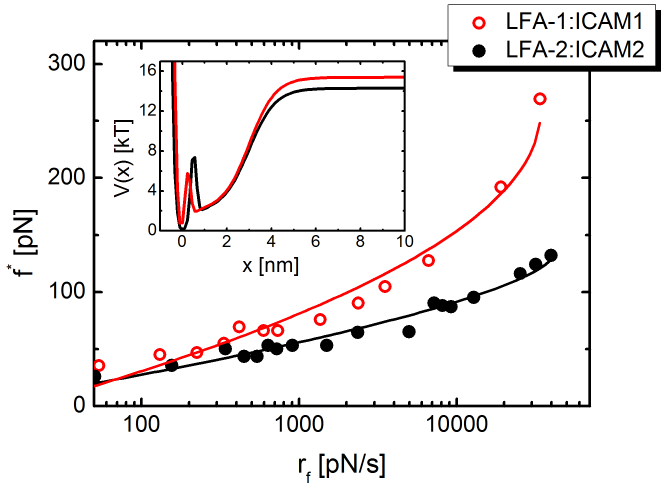


Figure 2: Fitting of dynamic force spectroscopy experiments for LFA-1:ICAM-1 and LFA-1:ICAM-2 complexes taken from [2] to Eq. (3) in main text. *Inset*: Proposed free energy profile for such complexes according to previous fitting.

main text, we consider more appropriate the proposed protocol, and thus we reinterpret the data in this context.

Figure 2 shows unbinding force data for LFA-1:ICAM-1 and LFA-1:ICAM-2 taken from [2] and fitted to Eq. (3) of main text. This allows us to obtain the free energy barrier height and position, yielding LFA-1:ICAM-1: $\Delta G^\dagger = 8.57 \pm 0.42 k_B T$ and $x^\dagger = 0.18 \pm 0.01 nm$ and LFA-1:ICAM-2: $\Delta G^\dagger = 7.57 \pm 0.38 k_B T$ and $x^\dagger = 0.40 \pm 0.01 nm$. Inset shows the proposed free energy profile according to our model and the obtained magnitudes.

Data for Biotin:Streptavidin and Biotin:Avidin complexes is taken from [3] although originally published in [4]. Here, due to the vast range of unfolding rates employed, one would see a clear deviation from Eq. (3) at lowest rates. As mentioned in the main text, this might be an effect of the second smooth slope, which starts to be "seen" by the experiment due to the extremely low pulling velocities.

## 6 Goodness of fit and model selection.

In the main text we show the results of the experimental data fit to equation (1) in three different cases: Bell-Evans model ($\nu = 1$ and two fitting parameters) and two more complex models ($\nu = 1/2$ and $\nu = 2/3$ and three fitting parameters). A first approach to the goodness of the fit is to evaluate the $\chi^2$ parameter which is an usual output of main statistic programs. However, as both kind of models have different number of fitting parameters a better measure of its increasing complexity is needed in order to compare the performance of different models. In the table (2) of the main text we write down the *reduced* $\chi^2$ which is defined as the ratio of the $\chi^2$ and the number of fit degrees of freedom ($n_{dof} = n - k$ , where $n$ is the number of data and $k$ the number of parameter of the model). Although this quantity takes into account the number of parameters $k$, other quantities have been proposed, like the Akaike (AIC) or Bayesian (BIC) information criterion, that rigorously discriminate between different models [5]. We have also computed and include in table (2) of the paper the result of the BIC of each model.

The BIC or Schwarz criterion is defined by [6]:

$$BIC = -2 \log L + (k+1) \log n, \tag{6}$$

where $L$ is the maximum likelihood of the fit. A simple commonly used approach to the calculus of the BIC is given by $BIC = n + n\log 2\pi + n\log(RSS/n) + (k+1)\log n$ with $RSS$ the residual sum of squares, which is directly proportional to the usually computed $\chi^2$. Thus maximum likelihood criterion corresponds to minimum $\chi^2$. BIC introduces a penalty of $\log n$ for each additional fitting parameter of the model. The model with lowest value of BIC is the best model from the data statistics point of view. BIC has been proved to be in many cases an effective approach to solve the model selection problem. However, a couple of caveats should be mentioned here: BIC is suitable for number of data $n$ much larger than the number of parameters in the model $k$; and BIC generally penalizes free parameters more strongly than other criteria.

## 7 Fit of numerical data to other theories

In the manuscript we have fitted the experimental data to Eq. (1) (main text) using three values for the exponent $\nu$. This theory considers that the barrier decreases as $(1 - f/f_c)^{1/\nu}$, being $f_c$ the critical force, $f_c = \Delta G^\dagger/\nu x^\dagger$. Here, $\nu = 2/3$ correspond to a cubic potential, which is a reasonable choice as any analytical potential can be expanded to a cubic polynomial next to the rupture force (for intermediate forces, as the ones found here).

Regarding the numerical data, in Fig. 5 of the manuscript only results for the fitting to the $\nu = 2/3$ exponent are shown However, in order to study the validity of the the different theories we can compare predictions for $\Delta G^\dagger$ and $x^\dagger$ to the correct values for a well-known, although non trivial, potential profile, as the one described in the Eq. (1) of this SI. This analysis is done in the table and in Figure 3. It shows small differences between ($\nu = 2/3$ and $\nu = 1/2$, though the first theory describes in a better way the barrier dependence $\Delta G(F)$. Note that Bell-Evans theory, $\nu = 1$, does not allow for obtaining a prediction for $\Delta G^\dagger$.

Being the force barrier dependence the main factor in the theory, we show in Figure 3 the dependence of the barrier with the force as numerically obtained for the proposed model and predicted for the two theories. It can be seen that the $\nu = 2/3$ is better for a wide range of force values.

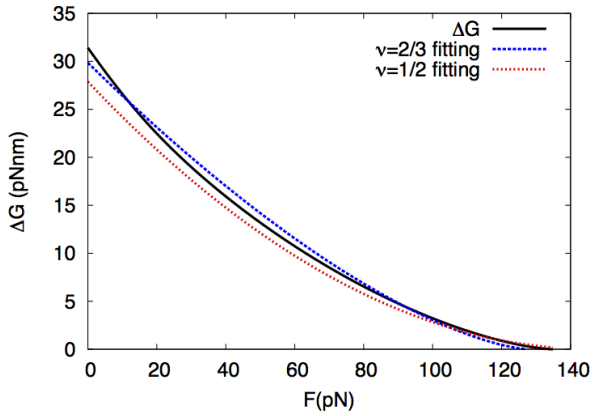


Figure 3: Barrier decreasing as a function of the applied force for our model potential [Eq. (1)], and for DFS theory with $\nu = 2/3$ and $\nu = 1/2$.

Table 1: Potential parameters $\Delta G^{\dagger}$ and $x^{\dagger}$ and reduced $\chi^2$ and $R$ parameters.

| | $\Delta G^{\dagger}(k_BT)$ | $x^{\dagger}(nm)$ | $\chi^2/R^2$ |
|---|---|---|---|
| Model | 7.70 | 0.50 | - |
| Fit: $\nu = 2/3$ | $7.28 \pm 0.2$ | $0.35 \pm 0.08$ | 0.06/0.996 |
| Fit: $\nu = 1/2$ | $6.80 \pm 0.14$ | $0.38 \pm 0.03$ | 0.08/0.997 |

## 8 Validation of the analysis protocol

For the sake of consistency, we probe our analysis protocol on the physical model using four different parameter sets. Figure 4 (left) shows the profiles for each of the four chosen parameter sets. In order to proof that our analysis procedure allows obtaining both $\Delta G^{\dagger}$ and $\Delta G^0$, the profiles have four different dissociation free energies $\Delta G^0$ but just two different barrier heights $\Delta G^{\dagger}$. This fact guaranties that the obtention of both free energy magnitudes from the same force data is completely independent.

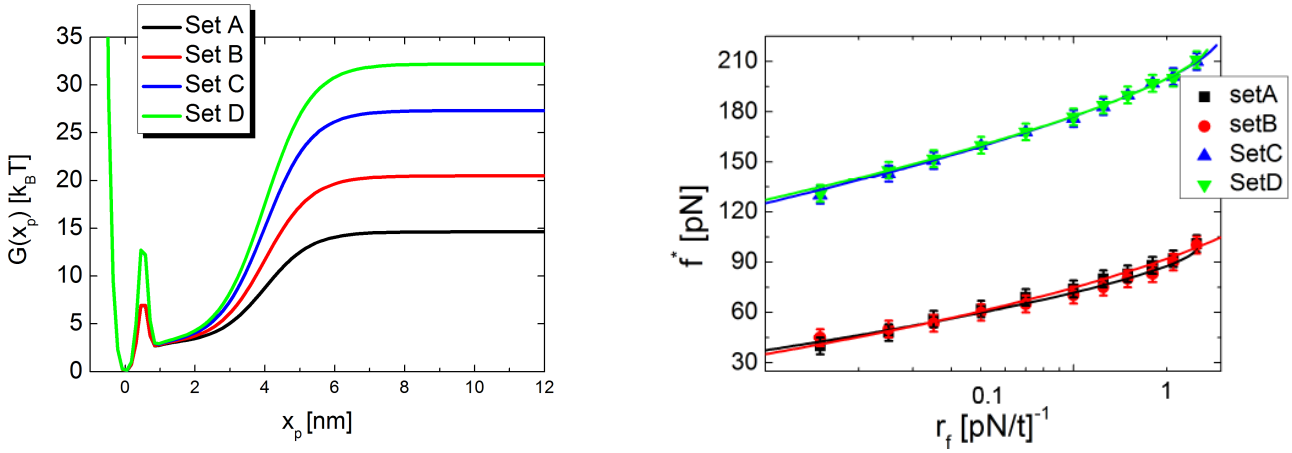


Figure 4: Left: Free energy profiles for the four chosen free energy profiles. All show different $\Delta G^0$ values bur barriers are equal in sets A-B and C-D respectively. Right: Typical rupture force $f^*$ versus pulling rate $r_f$ for the four parameter sets. Solid lines are fittings to Eq. (3) in main text.

We plot in Fig. 4 (right) the typical rupture forces versus the pulling rate for each of the four parameter sets. We can check how the curves corresponding to sets A-B and C-D superimpose respectively, as the profile has the same barrier height. The four data sets fit perfectly to expression (3) in the main text. Fitted parameters $\Delta G^{\dagger}$ are shown in Table I below.

Figure 5 shows the Jarzynski estimator $\Delta G^0_J$ as a function of the inverse of the pulling rate $r_f^{-1}$. Dashed lines indicate the dissociation free energy $\Delta G^0$ set on each of the four parameter sets. We can see clear convergence of each data set to their respective $\Delta G^0$ values, revealing that Jarzynski equality allows recovering the dissociation free energy successfully.

Table I gathers the $\Delta G^{\dagger}$ and $\Delta G^0$ values set for the four profiles together with the estimations from Jarzysnki equality $\Delta G^0_J$ and force spectroscopy theory $\Delta G^{\dagger}_f$ respectively. Indicated $\Delta G^0_J$ is the average of the last three values shown in Fig. 5 for each parameter set.

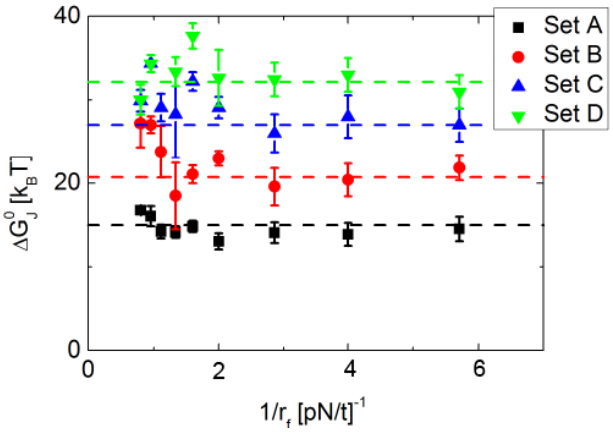


Figure 5: Jarzynki estimator $\Delta G_J^0$ obtained from simulation performed for each parameter set. Dashed lines indicate the values set for each parameter set $\Delta G^0$.

Table 2: Free energy magnitudes $\Delta G^0$ and $\Delta G^\dagger$ set for each parameter set and estimation according to our analysis protocol $\Delta G_J^0$ from Jarzynski equality and fitted $\Delta G^\dagger$.

| Parameter Set | $\Delta G^0(k_BT)$ | $\Delta G^\dagger(k_BT)$ | $\Delta G_J^0(k_BT)$ | $\Delta G_f^\dagger(k_BT)$ |
|---|---|---|---|---|
| A | 14.6 | 7.7 | $13.9 \pm 0.5$ | $7.3 \pm 0.3$ |
| B | 20.5 | 7.7 | $20.3 \pm 1.0$ | $6.7 \pm 0.5$ |
| C | 27.3 | 14.1 | $24.6 \pm 0.3$ | $13.2 \pm 0.6$ |
| D | 32.2 | 14.1 | $32.7 \pm 1.5$ | $12.5 \pm 0.4$ |

## 9 Effective stiffness

DFS analysis is based in Eq. (1) in the main text which is obtained after several approaches. Thus, this equation is obtained in the so-called weak spring limit of the system where $K_M \gg K_L, K_C$. Deviations from this case have been previously studied in [7, 8] for instance. Another approach concerning the stiffness of the system is to assume a constant $K_{\text{eff}}$, thus neglecting the force dependence of the effective stiffness of the system (which comes mostly from the $K_L$ term, the PEG is not a linear spring) [9]. With these caveats Eq. (1) can be used to analyze data and a well defined pulling rate $r_f = K_{\text{eff}} V$ is defined. Note here that from a theoretical perspective it would be natural to use the well controlled pulling velocity $V$ as control parameter of the system instead of the pulling rate $r_f$. However, following the tradition in the literature on the subject, we have decide to present our results in terms of $r_f$. Thus, in our work, we use a constant value of $K_{\text{eff}} = 10\text{pN/nm}$. We could question the validity of this approximation, then we should point two crucial facts (i) Theory is *validated* by our numerical simulations. We use the same approach to study the numerical simulations. There, the barrier parameters obtained by the DFS analysis show good agreement to the correct values. It shows the degree of robustness and accuracy of the employed theories. (ii) The error associated to neglecting the $K_{\text{eff}}(F)$ dependence is similar (same order of magnitude) to the one introduced by two other unavoidable approximations under the theory: the assumption of an specific form for the force dependence of barrier and prefactor in the Kramers rate expression, which are at the core of Eq. (1) result. To finish, this is the price to pay in order to have a simple useful result as Eq. (1).

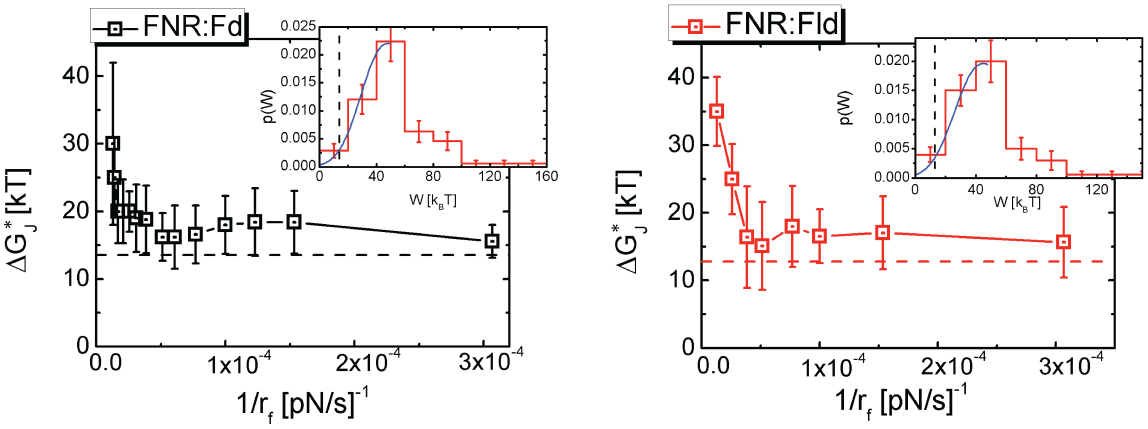


Figure 6: Corrected Jarzynski estimators by the bias estimation obtained fitting the work distributions (blue solid lines in the insets).

## 10 On the convergence of Jarzynski estimator

The Jarzynksi estimator for a finite number of $N$ irreversible work measurements $W_i$ can be written as:

$$\Delta G_J = -\log\left[\frac{1}{N}\sum_{i=1}^{N}\exp\left(-\frac{W_i}{k_B T}\right)\right], \tag{7}$$

where $k_B$ is the Boltzmann constant and $T$ the absolute temperature. Although it is an unbiased estimator when $N \to \infty$, in practice it suffers from poor convergence and it is highly biased when the system is too far from equilibrium. Efforts have been made on developing analytical theories to correct the bias for finite $N$. In particular, under conditions of high dissipation, Ref. [10] proposes the following expression for the bias of the Jarzynski estimator:

$$B_N = \mu + \log N - \Omega(\log N)^{1/\delta} - \lambda^{(1-\delta)/\delta}\left[\gamma + \frac{1-\delta}{\delta}\log(\log N) + \log\frac{q}{\delta}\right], \tag{8}$$

where $\gamma_E = 0.5772\cdots$ is the Euler-Mascheroni constant and $\Omega$ and $\delta$ are parameters given by fitting the work distribution left tail to the following expression:

$$P(W) = \frac{q}{\Omega}\exp\left[-\left(\frac{|W - W_M|}{\Omega}\right)^{\delta}\right], \tag{9}$$

where

$$\mu = (\delta - 1)\left(\frac{\Omega}{\delta}\right)^{\delta/\delta-1}, \qquad \lambda = \log N\left(\frac{\delta}{\Omega}\right)^{\delta/\delta-1}, \tag{10}$$

and $q$ is a normalization constant. Then the corrected Jaryzinski estimator is simply $\Delta G_J^* = \Delta G_J - B_N$.

In the case studied here, as mentioned in the main text and shown in Fig. 4, higher pulling rates lead to an overestimation of the free energy, due to the mentioned issues. Nonetheless, lowest rates meet the agreement between being close enough to equilibrium and having enough statistics to reach a well-converged Jarzynski estimator.

However, we calculate now the estimation of the bias shown in Eq. (8) to the work distributions showing high dissipation and thus being intrinsically biased. Figure 6 shows the

corrected Jarzynski estimator $\Delta G^*$ with an example of two work distributions fitted to Eq. (9) (insets), where the dashed vertical lines are the respective free energy values as obtained in the calorimetry experiments. Comparing with Fig. 4 in the main text, the free energy estimation is improved, specially in the intermediate rate region. Highest rates have a very poor estimation of the left tail (lower work values). Therefore, the fits to Eq. (9) are not meaningful, so is not the calculation of $B_N$.

## References


[1] Mossa A, de lorenzo S, Huguet JM, Ritort F (2009) Measurement of work in single-molecule experiments. *J Chem Phys* 130: 234116.

[2] Wojcikiewicz W, Abdulreda M, Zhang X, Moy VT (2006) Force spectroscopy of LFA-1 and its ligands, ICAM-1 and ICAM-2. *Biomacromolecules* 7:3188-3195.

[3] Hyeon C, Thirumalai D (2012) Multiple barriers in forced rupture of protein complexes. *J Chem Phys* 137:055103.

[4] Merkel R, Nassoy P, Leung A, Ritchie K, Evans E (1999) Energy landscapes of receptor-ligand bonds explored with dynamic force spectroscopy. *Nature* 397:50.

[5] Wit E, van den Heuvel E, Romeijn J-W (2012) 'All models are wrong ...': an introduction to model uncertainty. *Statistica Neerlandica* 66, 217-236.

[6] Schwarz G, (1978) Estimating the dimension of a model. *The annals of Statistics* 6, 461-464.

[7] Tshiprut Z, Klafter J, Urbakh M (2008) Single-molecule pulling experiments: when the stiffness of the pulling device matters. *Biophys. J.* 95: L42.

[8] Maitra A, Arya G (2010) Influence of pulling handles and device stiffness in single-molecule force spectroscopy. *Phys Chem Chem Phys* 13:1836.

[9] Ray C, Brown JR, Akhremitchev BB (2007) Rupture Force Analysis and the Associated Systematic Errors in Force Spectroscopy by AFM. *Langmuir* 2007, 23, 6076-6083.

[10] Palassini M.; Ritort F. *Phys. Rev. Lett.* **2011**, *107*, 060601.